MOLEKUL
eISSN: 2503-0310

Articles
https://doi.org/10.20884/1.jm.2023.18.2.6431

Synthesis, Characterization, and Antibacterial Activity Test of Geothermal Silica/$AgNO_3$ Thin Film

Yayuk Astuti*, R.A. Yunita Suci Rahayu, Arnelli

Chemistry Department, Faculty of Sciences and Mathematics, Universitas Diponegoro, Tembalang Semarang 50275, Indonesia

*Corresponding author email: yayuk.astuti@live.undip.ac.id

Received July 25, 2022; **Accepted** May 09, 2023; **Available online** July 20, 2023

ABSTRACT. Geothermal silica waste offers convenient, economical, and environmentally friendly material with high hydrophobicity to produce thin films. Silica-thin films from geothermal waste using the sol-gel method, though, no addition of $AgNO_3$ was conducted for antibacterial functions. This study aims to produce silica-thin films from geothermal waste with the addition of $AgNO_3$ and analyze the antibacterial activity. The procedures carried out in this research were (i) an acid leaching process using HNO_3; (ii) the production of silica thin film with and without the addition of $AgNO_3$; (iii) thin film characterization including a water contact angle measurement (WCA), XRF, FTIR, XRD and SEM-EDX on silica thin film samples with and without the addition of $AgNO_3$; and (iv) antibacterial activity test. The results show the optimum HNO_3 concentration for the acid leaching process was 20%, yielding 99.08% SiO_2 by mass. The WCA of the silica thin film in the presence and absence of $AgNO_3$ reached a value of ±160°, indicating the addition of $AgNO_3$ did not decrease the contact angle of the silica thin film. This research employed smart deconvolution of IR Spectra using Fityk software which reveals a higher area ratio for Si-O-Si relative to Si-OH. Furthermore, it was observed that the silica thin films exhibited an amorphous morphology, both without and with the addition of $AgNO_3$, with Ag discovered to be dispersed on the thin film. However, despite the presence of Ag, both TF20 and TF20+Ag samples were found to be ineffective in inhibiting bacterial growth, as evidenced by bacteria-free zones on the samples.

Keywords: $AgNO_3$, Geothermal Silica, Thin Film

INTRODUCTION

Semiconductor metal oxide thin films have risen in popularity due to their properties and diverse applications (Shinde et al., 2020). Thin films are materials with thicknesses ranging from micrometers (μm) to nanometers (nm), with a maximum thickness of about one millimeter (Fayomi et al., 2019). To name a few, thin films are used as anti-reflection coatings, mirrors, filters (Kasap & Capper, 2017), semiconductors in electronic devices, energy, and optoelectronic applications, as well as for wear, corrosion, and abrasion resistances (Fayomi et al., 2019).

Silica thin films are known to be used as hydrophobic coatings on glass (Darmawan et al., 2018). Various silanes can be used as starting materials for the manufacture of silica thin films, some of which are tetraethoxysilane (TEOS) (Yan et al., 2017; Sumardi et al., 2021; Kiomarsipour et al. 2023), ethyltriethoxysilane (ETOS) (Ramezani et al., 2015), and methyltrimethoxysilane (MTMS) (Darmawan et al., 2018; Gao et al., 2020; Esfahani et al., 2022). However, these materials have low hydrophobicity and are not effective for industrial scale as they are expensive (Purnomo et al., 2018). Alternative materials that offer more simple and economical processing, as well as high hydrophobicity, are, thus, needed to produce such thin films. Accordingly, silica can be acquired from geothermal waste (Purnomo et al., 2018). Geothermal silica is abundantly available as a by-product or waste from the geothermal power plant (Jenie et al., 2018).

Characterization of the hydrophobicity of silica thin films can be carried out using a contact angle measurement. The contact angle is the angle at which the liquid/vapor interface meets the solid. If the fluid used is water, the contact angle measured is the "water contact angle" (WCA). Thin film is categorized as hydrophilic if it has a WCA of less than 90°; whereas it will be hydrophobic if it has a WCA of more than 90°. Thin film surfaces with WCA > 150° have superhydrophobic properties; whereas surfaces with WCA < 10° have super hydrophilic properties (Sethi & Manik, 2018).

The silica applied to produce the thin films is acquired from geothermal waste through an acid-leaching process to remove inorganic impurities (Purnomo et al., 2018). The acids commonly used for the acid-leaching process include HCl (Darmawan et al., 2018), HNO_3 (Javed et al., 2018), and mixed acids (Khalifa et al., 2019). Thin films from geothermal silica are known to have no antibacterial

properties. One of the precursors that can be added to the silica thin film material to produce an antibacterial effect is $AgNO_3$. Silver has been known to have antibacterial properties since ancient times. Many new industries are involved in the production of antibacterial gels using silver nanoparticles (Lanje et al., 2010). Based on the research of Jeon et al. (2003) on Ag-SiO_2 thin film, silver inhibited the growth of bacteria by 99%.

The silica-thin film was synthesized by the sol-gel method (Darmawan et al., 2018). The sol-gel method was chosen because it requires low processing temperature, produces homogeneity in the coating, allows easy control over metal concentration and coating thickness, and allows the addition of reducing and oxidizing agents in small concentrations (Li et al., 2003). Purnomo et al. (2018) have previously produced thin silica from geothermal silica using the sol-gel method. However, the thin film was only produced as a coating for glass, bamboo, and zinc, and no addition of $AgNO_3$ was undertaken to create an antibacterial effect.

The present research focuses on the manufacture of geothermal silica-based thin film with the addition of $AgNO_3$ using the sol-gel spray coating method and its antibacterial activity. The silica-thin film generated was used as a superhydrophobic and antibacterial glass coating. The acid-leaching process in the geothermal silica purification process used nitric acid (HNO_3) at various concentrations to determine the optimal concentration indicated by the highest SiO_2 content.

EXPERIMENTAL SECTION

Materials

The materials used in this research were geothermal silica waste obtained from PT GeoDipa Dieng, Central Java, 65% HNO_3 solution (Merck), trimethylchlorosilane (TMCS) (Merck), $AgNO_3$ (Merck), Isooctane (Merck), 70% alcohol, nutrient agar (Merck), peptone (Merck), yeast (Merck) and distilled water. Silica thin film was used as a glass coating.

Geothermal Silica Waste Purification

Purification of geothermal silica waste followed the procedure of Purnomo et al. (2018) and Afriani et al. (2019). Purification of geothermal silica waste was undertaken by leaching using 65% HNO_3. First, 5 g of geothermal silica waste sieved to 150 mesh was added into 50 mL of HNO_3 in various concentrations of 15%, 20%, and 25%. The geothermal silica and nitric acid mixture were stirred and heated at a speed of 600 rpm and temperature of 80 °C for 3 hours. The mixture was then left overnight and washed using distilled water until the pH constant. Subsequently, it was filtered using Whatman 42 filter paper. The residue was then dried in an oven at 110 °C for 3 hours to reduce the water content in the silica. Further, the purified silica involving 15, 20, and 25% HNO_3 were denoted as SF15, SF20, and SF25, respectively.

Silica Thin Film Production with and without the Addition of $AgNO_3$

The production of silica thin films with and without the addition of $AgNO_3$ followed the research procedure conducted by Gurav et al. (2015) and Purnomo et al. (2018). SF15, SF20, and SF25 were used as the base materials in the production of thin films without the addition of $AgNO_3$. First, 30 mL of isooctane was added to 1.5 g of SF15 and stirred for 10 minutes at 500 rpm. The mixture was then sonicated for 15 minutes. TMCS was added slowly into the mixture whilst being stirred at 500 rpm and heated at a temperature of 50 °C for 1 hour, followed by sonication for 1 hour and a one-night-long aging process. Thin films made from SF20 and SF25 were produced using the same procedure. Furthermore, $AgNO_3$ incorporated silica thin film was made using SF20. The steps involved the procedure for silica thin film production without $AgNO_3$, to which, after the addition of TMCS, 0.051 grams of $AgNO_3$ was added whilst being stirred at a speed of 500 rpm and kept at a temperature of 50 °C for 1 hour. The steps were followed by sonication for 1 hour and aging for 1 night to achieve gel formation.

The resulting products were spray-coated onto a glass surface (Microscope glass slides, SAIL BRAND cat. no 7101; 25.4 x 76.2 mm, thickness 1mm – 1.2 mm). The thin films were spray-coated onto a glass surface following the procedure carried out by Saputra et al., (2018), i.e., with calcination at a temperature of 300 °C for 2 hours. The spray-coating and calcination processes were repeated 3 times to obtain an even surface of the thin film and prevent surface cracks. The silica-thin films without the addition of $AgNO_3$ from SF15, SF20, and SF25 were denoted as TF15, TF20, and TF25, respectively. The silica thin film with $AgNO_3$ from SF20 was denoted as TF20+Ag.

Silica Xerogel Production with and without the Addition of $AgNO_3$

The silica gels with and without the addition of $AgNO_3$ which had been kept overnight were filtered using Whatman 42 filter paper. The residues were put in an oven at 60 °C for 1 hour to reduce water content. They were then calcined in a furnace at 300 °C for 2 hours. The silica xerogels produced without the addition of $AgNO_3$ from SF15, SF20, and SF25 were denoted as XF15, XF20, and XF25, respectively. The silica xerogel with the addition of $AgNO_3$ from SF20 was denoted as XF20+Ag.

Characterization

SF15, SF20, and SF25 were characterized using X-Ray Fluorescence (XRF) "Rigaku Supermini 200 Voltage 40kV" (USA) to determine the elemental content before and after purification of the geothermal silica. Samples XF15, XF20, XF25, and XF20+Ag were analyzed using a Fourier-Transform Infrared Spectrometer (FTIR) (Shimadzu IRAffinity-1 (Japan) at a wavenumber of 4000 – 400 cm^{-1} and rate of 0.25 cm^{-1} at room temperature) for the presence of

functional groups identification in the silica thin film and X-Ray Diffraction (XRD) (Shimadzu 7000 (Japan) with 2θ measurement using Cu-Kα radiation (λ = 0.15406 nm)) to determine crystal structure the formed silica thin film. Morphology and chemical composition was performed on XF20+Ag using SEM Jeol JED 6510LA at 20 kV (Japan) at 200x, 500x, 1000x, and 5000x magnifications. Contact angle measurement was performed on samples TF15, TF20, TF25, and TF20+Ag to determine the hydrophobicity of the thin films. The surfaces of the silica thin films were dripped with a few drops of solution using a syringe. The solution droplets were photographed using a Vivo Y12 camera with the help of a macro lens (Canon EF 100 mm macro, EF-S 18–55 mm). The solution used for contact angle measurement was methyl orange dissolved in distilled water. Methyl orange was used to acquire a clear optical image. The average contact angle value was obtained by measuring three contact angles at different points on the same thin film surface. The contact angle of the water droplet was measured based on the length and height as shown in the image captured. The contact angle was calculated using the following arc-tangent equations:

$$\tan \theta_1 = \left(\frac{h}{r}\right) \quad (1)$$

$$\theta = 2 \arctan \frac{h}{r} \quad (2)$$

where r = droplet radius, and h = water droplet height (Darmawan et al., 2018).

Antibacterial Activity Test

The antibacterial activity test was carried out using the disc diffusion method. The samples were tested against gram-positive *Staphylococcus aureus* (*S.Aureus*) bacteria and gram-negative *Escherichia coli (E.Coli)* bacteria. The bacterial stocks were obtained from the UNDIP Biochemistry Laboratory. A total of 0.05 g yeast, 0.25 g peptone, and 2 g nutrient agar were dissolved in 100 mL distilled water. The media solution and petri dish were sterilized using an autoclave for 45 minutes. All tools and materials were put in Lamin Air Flow (INNOTECH IBS H1100, Indonesia) with an air flow of 0.45 ms^{-2} and sterilized with UV light for about 10 minutes. The sterilized media was poured into five petri dishes at 20 mL each and allowed to solidify in Lamin Air Flow to keep them sterile. A total of 30 μL of a suspension of gram-negative bacteria, namely *E. coli*, and gram-positive *S. aureus* bacteria, were inoculated on the test media in petri dishes. The bacterial suspension was spread until evenly distributed. The samples used for the antibacterial test were XF20 and XF20+Ag solutions. 10 μL of each sample solution was dropped onto a 0.5 cm diameter paper disc. The wet disc paper was then placed on top of the test medium in its petri dish that had previously been inoculated with *E. coli* and *S. aureus* bacteria. Observations of bacterial inhibition zones were conducted at incubation periods for 8, 12, and 24 hours at 37 °C.

RESULTS AND DISCUSSION

Geothermal Silica Purification

Nitric acid (HNO_3) was used for leaching to dissolve heavy metals contained in the geothermal waste because the acid is corrosive (Silviana et al., 2020) and can dissolve heavy metals. Acid-leaching was carried out with various concentrations of HNO_3, namely 15, 20, and 25% to determine the optimum concentration for dissolving heavy metals contained in the geothermal waste effectively and obtain the highest SiO_2 content.

Table 1 presents XRF analysis results of geothermal silica before and after purification using HNO_3. As can be seen, SiO_2 content after purification increased due to the dissolution of heavy metals by nitric acid. The process entails the binding of NO_3^- to metallic elements to form nitrates, while H^+ binds oxygen to form water molecules (H_2O). Silicon dioxide is an acid oxide; a non-metallic oxide compound that binds oxygen and is difficult to dissolve in acids but easily soluble in bases. The addition of HNO_3 in the acid-leaching process was shown to be effective in cleaving metal bonds and yielding metal nitrates, that, in consequence, reducing heavy metal content in geothermal silica and increasing the silica content.

Table 1. XRF Data of Geothermal Silica Samples

Element (% mass)	GS	SF15	SF20	SF25
Al_2O_3	-	0.07	0.06	-
SiO_2	91.08	99.04	99.08	98.93
Cl	5.26	-	-	-
K_2O	2.02	0.16	-	0.16
CaO	0.63	0.08	0.08	0.08
Fe_2O_3	0.63	0.46	0.54	0.56
As_2O_3	0.08	0.02	0.02	0.02
Sb_2O_3	0.23	0.15	0.18	0.24
Rb_2O	0.02	-	-	-
Br	0.04	-	-	-

The mechanism of the dissolution reaction of metals by acid was proposed by Epstein et al. (1980), Ma et al. (2013), and Rogozhnikov et al. (2021) as can be seen in the following (**Figure 1**). The SiO_2 content in SF25 decreased, speculated to be attributed to saturation or a constant state of NO_3^- from HNO_3 (Safrianti et al., 2012), implying that the metal content increased; consequently, SiO_2 content decreased. Measurement of SiO_2 content (mass fraction, %) in the SF25 indicated that the optimum concentration of HNO_3 in dissolving metals was 20%. Research by Javed et al. (2018) regarding the optimization of HNO_3 leaching towards copper from AMD Athlon precursors also demonstrated an HNO_3 optimum concentration of 20%.

Silica Thin Film without $AgNO_3$

The fabrication of silica thin films without the addition of $AgNO_3$ was conducted by a sol-gel process through hydrolysis and condensation reactions with TMCS. The sol-gel process involved the reaction between silica and TMCS as proposed by Brinker and Scherer (2013) and Sarawade et al. (2010) as can be seen in the following reaction (**Figure 2**). **Figure 2** depicts the sol-gel reaction between silica and TMCS. The TMCS was used as a sillation agent that reacts with Si–OH to form $–OSi(CH_3)_3$ group through condensation. Silanol (SiOH) on the surface of the silica will react with $Si(CH_3)_3Cl$ or trimethylchlorosilane (TMCS) to form Si – O – Si groups which are siloxanes that contribute to the hydrophobic nature of the thin film. Once condensation had taken place, aging or gel formation followed for as long as one night. The sol-gel suspension formed was then coated onto glass using the spray.

Water Contact Angle of Silica Thin Film without $AgNO_3$

Measurement of water contact angle aims to determine hydrophobicity of glass surface before coating (BC) and after coating with silica thin film without $AgNO_3$ (TF15, TF20, and TF25).

$$Fe_2O_3 + 6HNO_3 \longrightarrow 2Fe(NO_3)_3 + 3H_2O \quad (3)$$

$$K_2O + 2HNO_3 \longrightarrow 2K(NO_3) + H_2O \quad (4)$$

$$CaO + 2HNO_3 \longrightarrow Ca(NO_3)_2 + H_2O \quad (5)$$

Figure 1. Reaction mechanisms of heavy metals with nitric acid

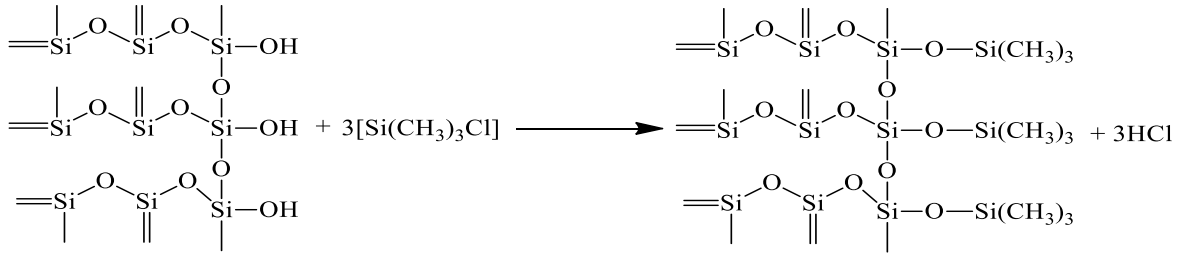

Figure 2. Silica-TMCS sol-gel reaction schematic (Sarawade et al., 2010)

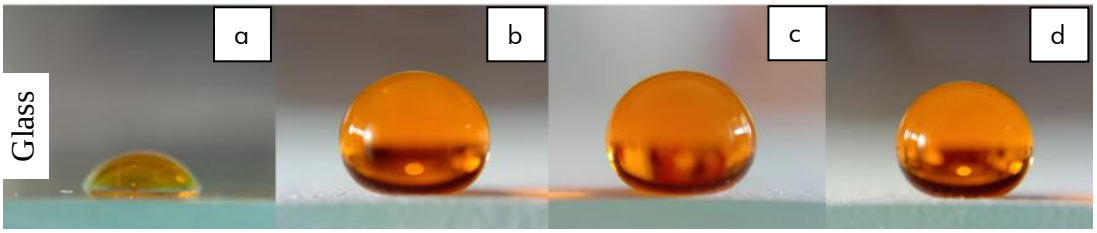

Figure 3. MO solution droplets on the surface of glass untreated and treated with silica thin film without $AgNO_3$ (**a**) BC; (**b**) TF15; (**c**) TF20; (**d**) TF25

Table 2. Water contact angles of silica-TMCS thin film-coated glass with calcination at 300 °C

Material	BC (°)	TF15 (°)	TF20 (°)	TF25 (°)
Glass	74.86	159.85	162.82	155.12

Figure 3(a) shows the flattened shape of the droplet on the uncoated glass. In contrast, **Figure 3(b)**,**(c)**, and **(d)**, depict the droplets atop the surface had rounder and more elevated spheres almost to a full circle, revealing that the glasses, which were coated with TF15, TF20, and TF25, are hydrophobic. Based on the images as shown above, water contact angles from all the glasses uncoated and coated with the silica-thin film without $AgNO_3$ were measured and the results are presented in **Table 2**.

Table 2 presents the contact angles measured from the glass treated with the silica thin film without the addition of $AgNO_3$ and calcined at a temperature of 300 °C. The untreated glass with the silica thin film had a hydrophilic surface as indicated by the contact angle of less than 90°. In contrast, treatment with silica thin film with no $AgNO_3$ as coating generated a glass surface with contact angles of more than 150° showing superhydrophobic character. The highest contact angle is achieved by TF20. Based on XRF analysis (**Table 1**), SF20 has the highest SiO_2 content compared to SF15 and SF25. The high SiO_2 in the SF20 sample might be attributed to an increase in Si-O-Si groups formed during the condensation reaction contributing to the hydrophobicity of the silica thin film, resulting in the highest contact angle.

Functional Group Characterization of Silica Thin Film Silica without $AgNO_3$

Typically, silica has an absorption peak at the wavenumber 1350-650 cm^{-1} due to the vibration of the main silicate network with its different bonding arrangements (Saputra et al., 2018). The absorption peak observed at 1000-1200 cm^{-1} corresponds to Si – O – Si asymmetric vibration and 800 cm^{-1} corresponds to Si – O – Si symmetrical vibration (Saputra et al., 2018). The absorption peak at 1600 cm^{-1} is denoted as the weak OH bending vibration of the silanol group (Li et al., 2012). **Figure 4** presents FTIR absorptions of geothermal silica (SG), TF15, TF20, and TF25.

Functional groups identified and their corresponding wavenumbers in the silica thin film samples without $AgNO_3$ are presented in **Table 3.** The SG sample has a Si-O-Si absorption peak from the silica structural network (Silviana et al., 2020). The absorption peak at the wavenumber 3445 cm^{-1} in SG indicates the presence of a strong O-H functional group, which is not identified in TF15, TF20, and TF25. Samples TF15, TF20, and TF25 do not have strong O-H functional groups indicating that with the addition of TMCS through hydrolysis and condensation processes, the OH in the silanol group will be replaced by Si from TMCS to form Si-O-Si bonds (siloxane) assumed to form hydrophobic properties of silica thin films. Despite this, TF15, TF20, and TF25 samples exhibit OH absorption peaks, implying that residual OH from the silanol groups and water remnants are still present (Sulejmanović et al., 2015). Based on FTIR characterization, no absorption peak was observed for the Si-Cl group, predicted to have been released in the dissolution stage and hydrolyzed by the solvent, thus, has no effect on the thin film structure (Darmawan et al., 2021).

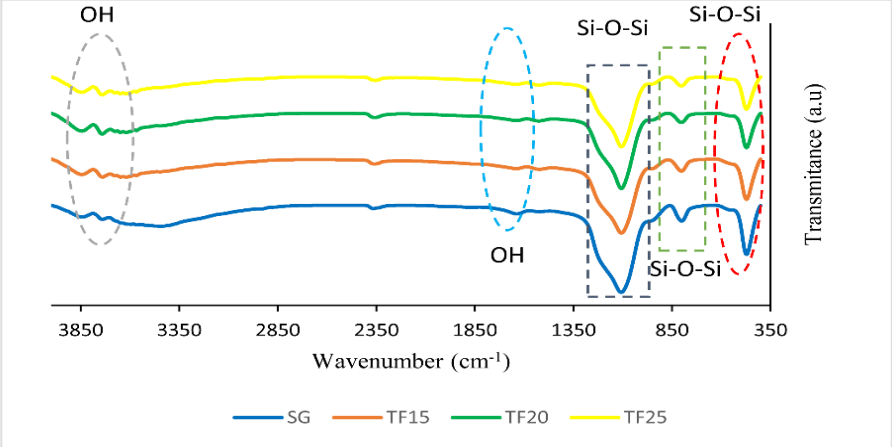

Figure 4. IR spectra of silica and silica thin films without the addition of $AgNO_3$

Table 3. Functional groups present in silica thin films without the addition of $AgNO_3$

Functional group	Wavenumber (cm^{-1})			
	SG	TF15	TF20	TF25
Si-O-Si Bending Vibration	471.7	471.81	471.7	471.51
Si-O-Si Symmetrical Vibration	800.65	801.8	801.85	801.64
Si-O-Si Asymmetrical Vibration	1107.41	1106.52	1106.64	1106.14
Silanol OH Bending Vibration (weak)	1637	1640.81	1524.86	1524.25
OH Stretching Vibration (strong)	3445.12	-	-	-
OH Stretching Vibration	3842.4	3843.11	3844.15	3843.93

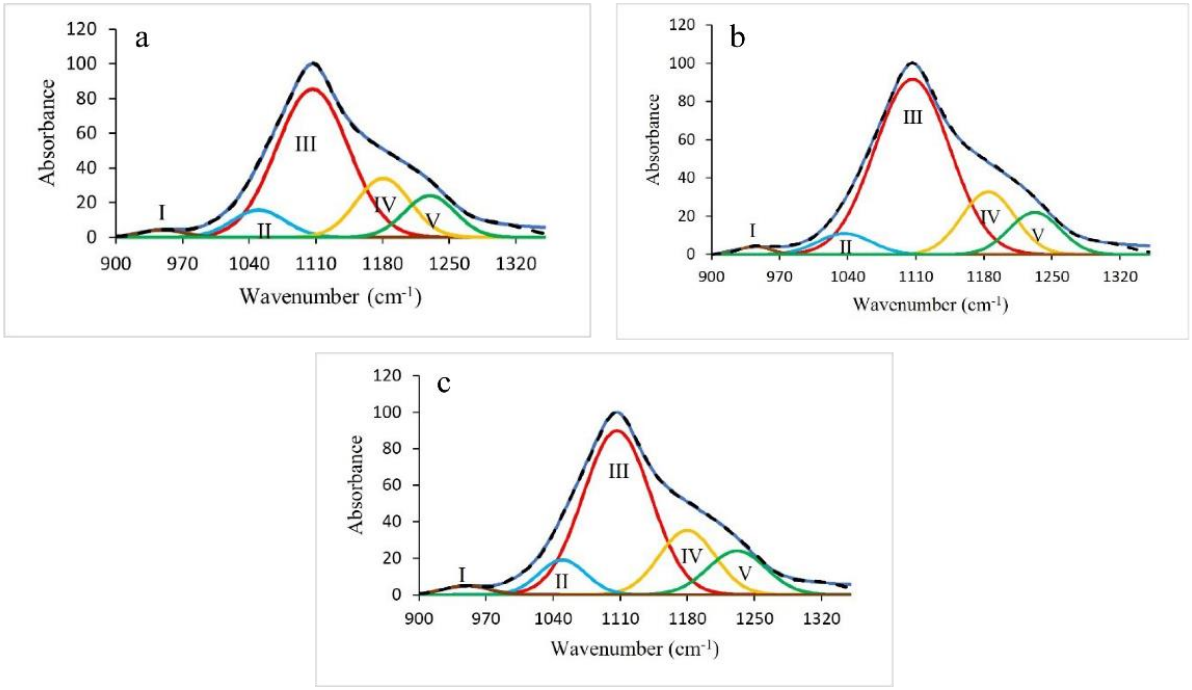

Figure 5. Deconvoluted spectra of silica thin film using Fityk at wavenumber 1350-900 cm^{-1} (**a**) TF15; (**b**) TF20; (**c**) TF25

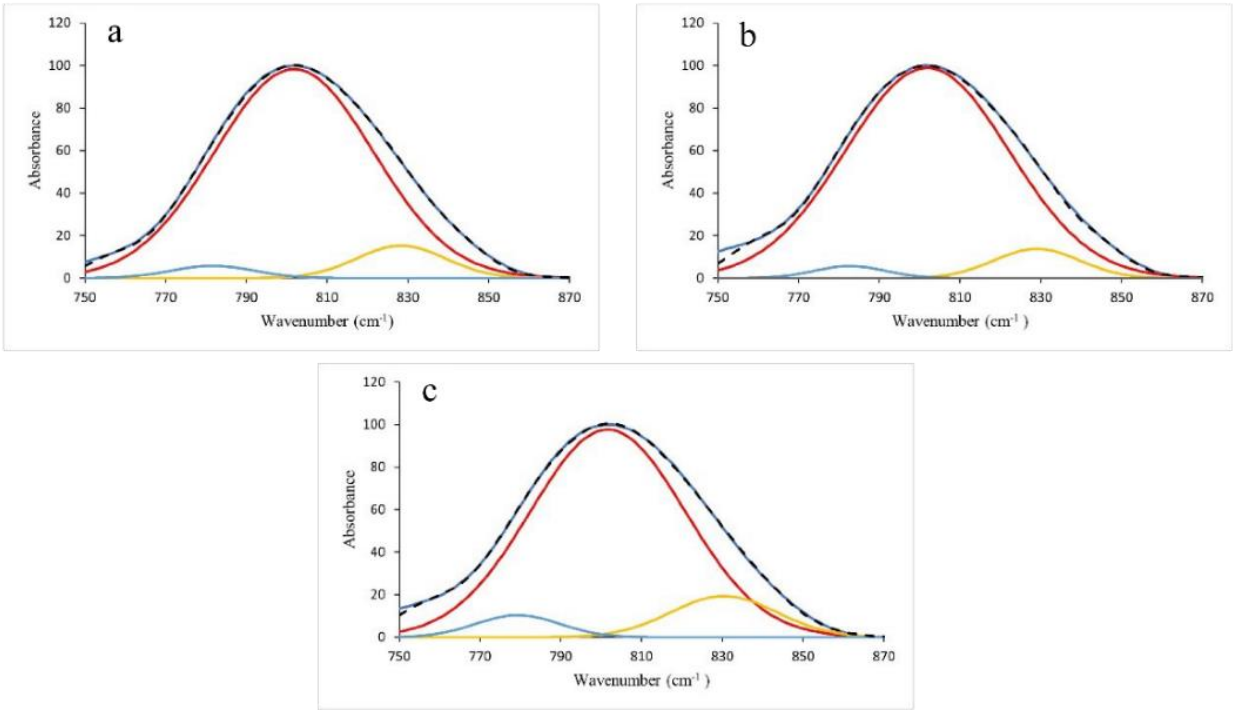

Figure 6. Deconvoluted spectra of silica thin films at wavenumber 870-750 cm^{-1} (**a**) TF15; (**b**) TF20; (**c**) TF25 computed using Fityk

Table 4. Si-O-Si and Si-OH vibrations absorption areas as determined using Fityk

Sample	Frequency (cm^{-1})			Area Ratio		
	v_{as} Si-O-Si	v_s Si-O-Si	v Si-OH	v_{as} Si-O-Si	v_s Si-O-Si	v Si-OH
TF15	1106.64	801.85	949	1.01	1.03	1.37
TF20	1106.64	801.85	949	1.11	1.07	1.00
TF25	1106.64	801.85	949	1.00	1.00	1.63

The wavenumber range of 1350-900 cm^{-1} is attributed to the stretching of the main silicate network. The area of each absorption region in samples TF15, TF20, and TF25 can be broken down into its comprising constituents and determined by spectral deconvolution using Fityk. **Figure 5** shows deconvoluted spectra of silica thin films of TF15, TF20, and TF25 samples computed using Fityk. The area I at wavenumber around 960 cm^{-1} is assigned to Si-OH vibration, area II at wavenumber around 1030 cm^{-1} is attributed to Si-O-Si linear vibration (Darmawan et al., 2021), area III at wavenumber 1106 cm^{-1} was the asymmetric vibration of Si-O-Si (Saputra et al., 2018), area IV at wavenumber 1180 cm^{-1} is assigned to the longitudinal optical (LO) vibration of Si-O-Si (Sulejmanović et al., 2015), and peak V at wavenumber around 1260 $cm^{-1}$is indicated the presence of the Si-OC and Si-CH_3 vibrations (Darmawan et al., 2021). From the deconvoluted spectra (**Figure 5**), Si-OH functional group is significantly smaller compared to Si-O-Si. The Si-OH functional group yields the hydrophilic nature of the silica thin films, whereas the Si-O-Si group yields the hydrophobic nature of the silica thin film. Accordingly, as observed from the IR absorptions, TF15, TF20, and TF25 are superhydrophobic as representative areas for Si-OH functional group in the samples and are significantly smaller than Si-O-Si. The group that affords the hydrophobic nature of thin film silica can be identified within 870 to 750 cm^{-1} of Si-O-Si symmetrical vibration (Saputra et al., 2018). Si-O-Si symmetrical vibrational absorption is also determined by spectral deconvolution using Fityk.

Deconvoluted IR spectra of TF15, TF20, and TF25 samples at wavenumbers 870-750 cm^{-1} are presented in **Figure 6**. The area of Si-OH and Si-O-Si vibrations are compared to determine which of the two in the TF15, TF20, and TF25 samples have the larger area which features the proclivity of the material towards hydrophilicity or hydrophobicity.

Table 4 presents the area ratios of the asymmetric and symmetrical Si-O-Si and Si-OH vibrations in silica thin films. Wavenumbers 1106 and 801 cm^{-1} signify asymmetric and symmetrical Si-O-Si stretching vibrations (Saputra et al., 2018) and 949 cm^{-1} signifies Si-OH vibrations (Darmawan et al., 2021). As can be seen, the TF20 sample has the largest Si-O-Si area ratio of both symmetrical and asymmetrical vibrations, and the smallest Si-OH area. The silanol group (Si-OH) yields hydrophilic properties and TF20 has the smallest Si-OH area. Hydrogen bonding with water is more difficult to establish with Si-O-Si or Si-O-Si$(CH_3)_3$ groups than Si-OH. Therefore, the large Si-O-Si functional group would increase the hydrophobic properties of the silica thin films. Results from the deconvolution are consistent with contact angle measurements (**Table 2**), whereby it is observed that TF20 has the highest contact angle, indicating its superhydrophobic properties.

Silica Thin Film with $AgNO_3$

SF20, with the addition of $AgNO_3$, is used to produce the silica thin films owing to its highest contact angle (**Table 2**). That is, the purified silica has the highest hydrophobicity among the other silica base materials obtained from geothermal waste.

Silica thin films synthesized via the sol gel method involve the addition of $AgNO_3$. The addition of $AgNO_3$ aims to enhance the antibacterial properties of the thin films. Jeon et al. (2003) carried out the production of silica thin films involving the addition of $AgNO_3$ using the sol gel method, demonstrated a 99.9% inhibition of bacterial growth. In this research, silica thin films with Ag were calcined at a temperature of 300 °C. The reaction taken between silica and $AgNO_3$ followed by Jeon et al. (2003) and is detailed in the following reaction (**Figure 7**). **Figure 7** is the schematic of the reaction between silica-TMCS with the addition of Ag. Illustrated in **Figure 2** of the sol-gel reaction between silica and TMCS and the absence of Ag, silanol residues not bound to –OSi$(CH_3)_3$ from TMCS were present. With the addition of $AgNO_3$, Ag would then bind to these silanols. Prior studies by Bruni et al. (1999), De et al. (1996), and Jeon et al. (2003) asserted the proclivity of Ag^+ to bind to Si-OH, that is the sol formed from hydrolysis. Ag^+ ions would enter the silica matrix and form Si-O-Ag.

Coating of the silica thin film with $AgNO_3$ was done for three times to achieve a flat surface and prevent cracking. **Figure 8** displays a glass surface that coated with the $AgNO_3$-incorporated silica thin film. The thin film surface was analyzed for its water contact angle as a measure of hydrophobicity parameter and characterized using FTIR and XRD.

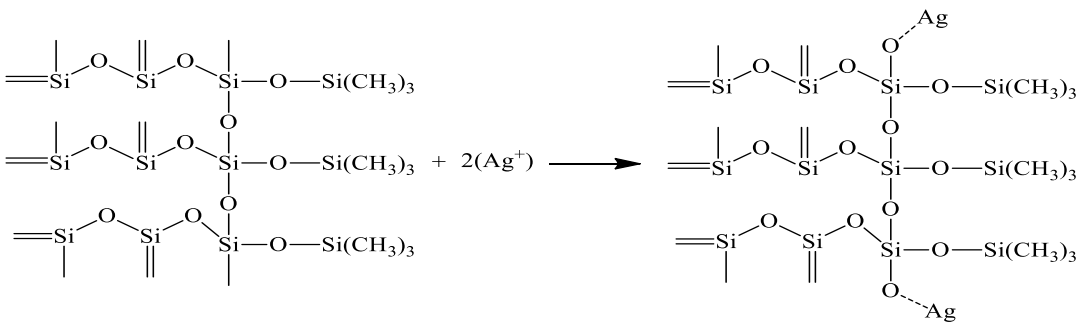

Figure 7. Silica-TMCS sol-gel reaction with the addition of Ag (Jeon et al. 2003)

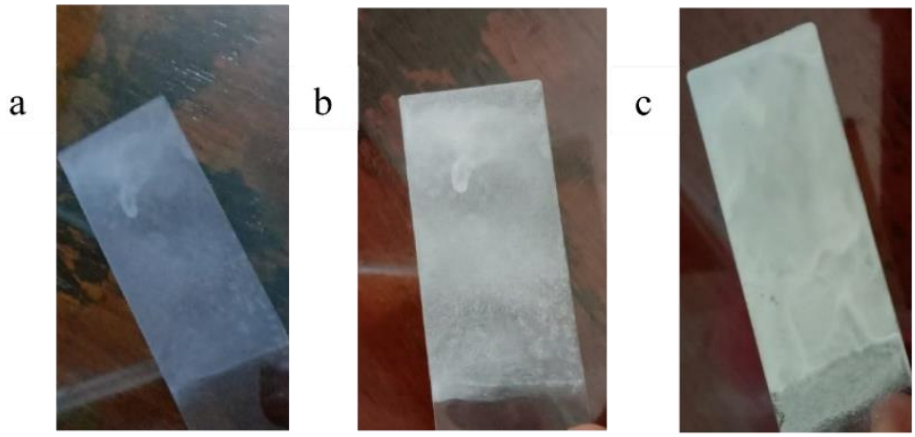

Figure 8. The Glass surfaces coated with silica thin film with $AgNO_3$ (**a**) 1 time coating (**b**) 2 times coating (**c**) 3 times coating

Contact Angle of Silica Thin Film with Addition of $AgNO_3$

The silica thin film with $AgNO_3$ (TF20+Ag) was assessed for its water contact angle to evaluate the effect of the addition of $AgNO_3$ on the hydrophobicity of the thin film formed. **Figure 9** displays droplets of MO solution on a TF20+Ag coated surface. The contact angle measured from the TF20+Ag coating is 163.83°, placing it in the superhydrophobic category as is more than 150°. In **Table 2**, the uncoated glass has a contact angle of 74.86° and TF20 has 162.82°. This implies that the addition of $AgNO_3$ to the silica thin film does not reduce the contact angle formed.

FTIR Characterization of Silica Thin Film with $AgNO_3$

Figure 10 shows the FTIR spectrum of the silica thin film with $AgNO_3$. The absorption peak at 471.06 cm^{-1} is denoted as the Si-O-Si bending vibration. The absorption peaks at 801.74 cm^{-1} and 1104.22 cm^{-1} are the symmetrical and asymmetrical vibrations of the Si–O–Si group (Darmawan et al., 2021). The absorption peak at 1628.46 cm^{-1} is the weak OH bending vibration of the silanol remnants in the thin film (J. Li et al., 2012). Absorptions at 3443.96 cm^{-1}, 3648.87 cm^{-1}, 3673.69 cm^{-1}, 3741.88 cm^{-1}, 3839.77 cm^{-1} are OH stretching vibrations from water (Sulejmanović et al., 2015).

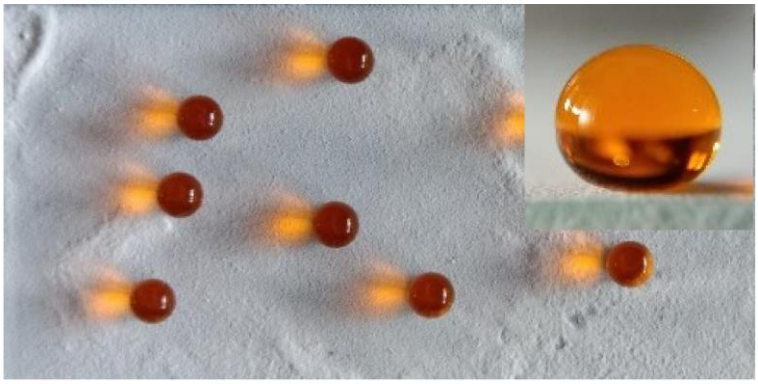

Figure 9. Droplets of MO solution on TF20+Ag

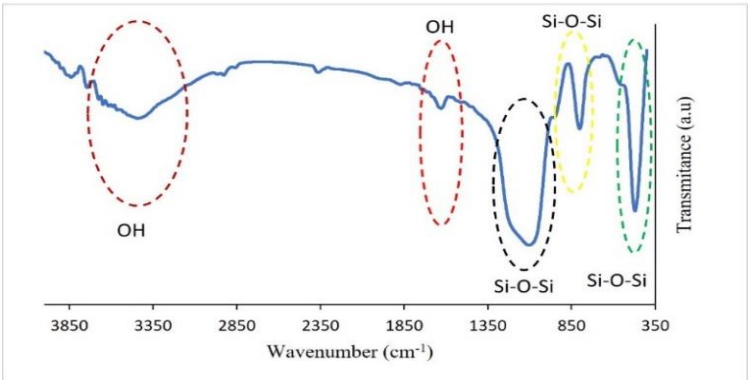

Figure 10. The IR spectrum of silica thin film with $AgNO_3$

XRD Characterization of Silica Thin Film with Addition of $AgNO_3$

Figure 11 shows the diffractograms of the TF20 and TF20+Ag samples. TF20 is amorphous with a broad peak centered at 2θ 25°. The presence of amorphous silica can be confirmed through a diffraction peak that widens at 2θ around 21-25° (Jenie et al., 2018; Muljani et al., 2014; Widiyandari et al., 2021). The XRD pattern of the TF20+Ag shows crystal attributes as well as a broadened peak of amorphous silica (21-25°). The 2θ diffraction peaks 55.04°, 46.42°, 32.46°, and 28.04° indicate the presence of a crystal structure of the AgBr. Based on the JCPDS database 96-901-1687, the AgBr has 2θ peaks at 55.01°, 46.42°, 32.46°, and 28.07°. The AgBr is formed anticipatedly from residual Br that exists as an impurity in the geothermal silica.

Morphology and Elemental Distribution of Silica Thin Film with $AgNO_3$

The TF20+Ag sample was analyzed using SEM and EDX to determine Ag distribution on the silica-thin film. The TF20+Ag xerogel sample was subjected to SEM analysis to obtain the surface morphology of the silica thin film. The SEM images of TF20+Ag are shown in **Figure 12**.

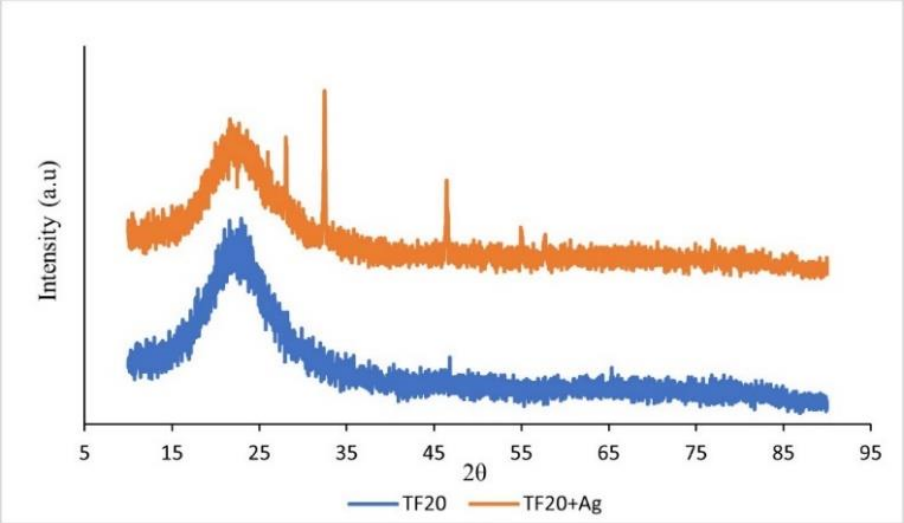

Figure 11. XRD diffractograms of TF20 and TF20+Ag

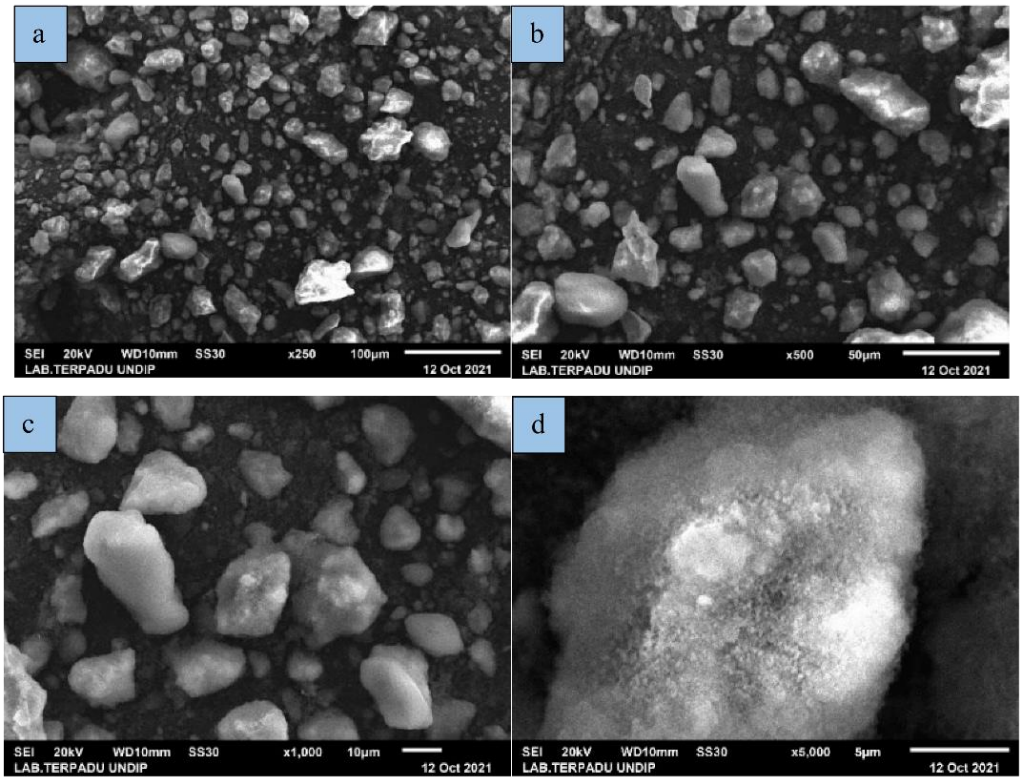

Figure 12. SEM images of TF20+Ag sample with(**a**) 250x (**b**) 500x (**c**)1000x (**d**) 5000x magnifications

Images in **Figure 12** show that the TF20+Ag sample has an elongated round shape where some are irregular. SEM images at 250x, 500x, and 1000x magnifications still show the various shapes of TF20+Ag, and at 5000x magnification, the surfaces are increasingly clear.

Figure 13 presents the amount of Ag contained in TF20+Ag. The EDX results show that the TF20+Ag sample contains metal oxides, namely SiO_2, at 42.78%. The high content of silica oxide in the thin film indicated that the thin film was made from geothermal silica. This is in line with XRD and FTIR data showing the presence of amorphous silica and Si-O-Si groups as illustrated in **Figure 10** and **Figure 11**. To highlight this, the composition and elemental distribution of TF20+Ag are shown in **Table 5** and **Figure 14**.

Table 5 elemental constituents of TF20+Ag are, namely, carbon, oxygen, silica, and silver. The elemental composition suggests that the silica thin film with $AgNO_3$ was successfully synthesized. The Ag element in TF20+Ag is tiny as the concentration of $AgNO_3$ added to TF20+Ag was low.

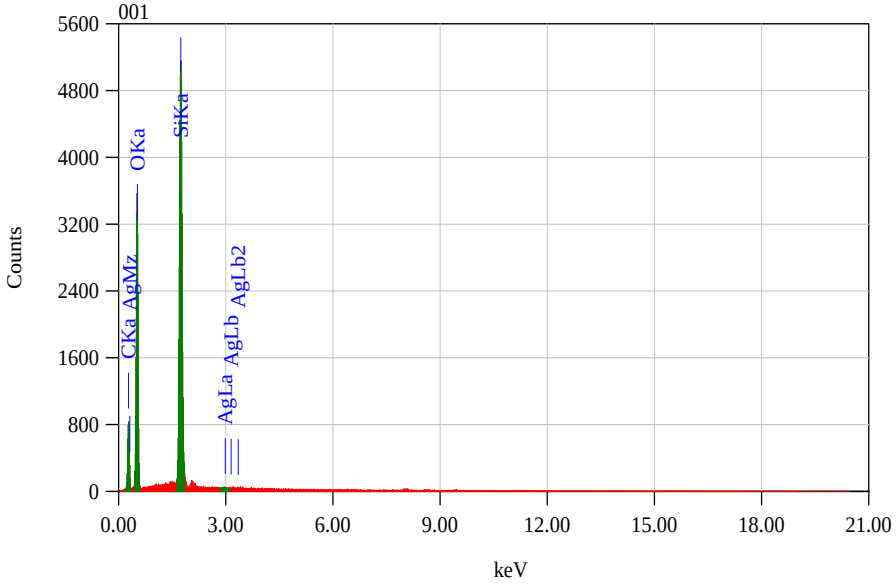

Figure 13. EDX spectrum of TF20+Ag

Table 5. Elemental composition of TF20+Ag

Element	Composition TF20+Ag (%)
C	57.03
O	22.80
Si	20.00
Ag	0.18

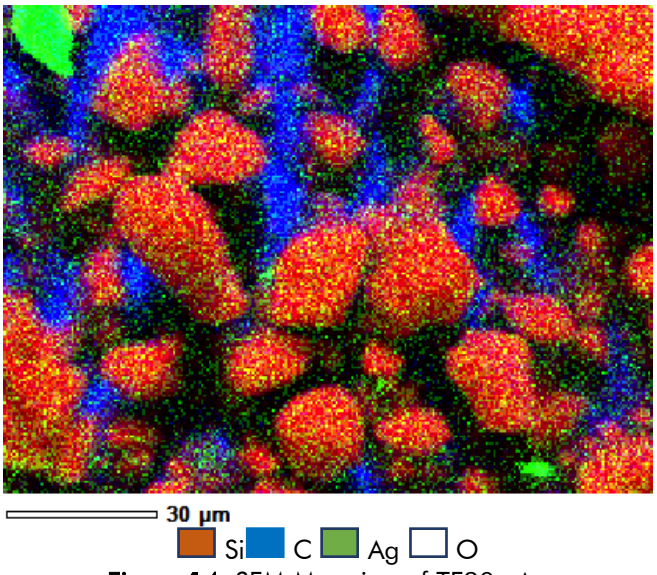

Figure 14. SEM Mapping of TF20+Ag

Table 6. Bacterial inhibition zone of silica thin films without and with the addition of $AgNO_3$

Sample	Inhibition zone (mm)			
	E. Coli		*S. Aureus*	
	8hrs	12hrs	8hrs	12hrs
TF20	-	-	-	-
TF20 + Ag	-	-	-	-
$AgNO_3$ 0.01 M	8	10	8	8
Control +	26	28	26	28
Control -	-	-	-	-

Figure 14 depicts the elemental distribution in TF20+Ag sample, revealing the presence of Si, C, O, and Ag elements. The TF20+Ag sample is shown to be dominated by Si and C elements. Ag is shown to be distributed evenly on the silica thin film material.

Antibacterial Activity

The antibacterial activity test was aimed to evaluate the effect of $AgNO_3$ addition on the silica thin film's antibacterial properties. $AgNO_3$ was added to provide antibacterial properties on the silica thin film as observed by Jeon et al. (2003) in which they produced Ag-SiO_2 thin film using $AgNO_3$ and the sol-gel method and was able to inhibit the growth of *E. Coli* and *S. Aureus* bacteria by 99.9%. Another study found that Ag/SiO_2 composite with Ag incorporated onto nano-sized silica sourced from $AgNO_3$ also inhibited the growth of *E. Coli* and *S. Aureus* bacteria (Sotiriou et al., 2011). In addition, the correlation between the hydrophobicity of the surface and antibacterial activity is that substrate wettability is the main factor influencing bacterial adhesion since the bacteria adhesion on the surface is mediated by surface wettability (Levana et al., 2022). Yuan et al. (2017) and Hemmatian et al. (2021) reported that surfaces with hydrophobic properties showed reduced bacterial attachment; on the contrary, hydrophilic surfaces increase bacterial adhesion. **Table 6** presents measurements of the inhibition zone indicative of bacterial activity of the silica thin films without and with the addition of $AgNO_3$.

Table 6 demonstrates that at 8 hours and 12 hours incubation, the TF20 and TF20+Ag samples have no inhibitory zone against gram-negative bacteria (*E. Coli*) and gram-positive bacteria (*S. Aureus*). This may be possible due to the very small and, thus, insufficient amount of silver particles on the silica surface. In this study, the incorporation of Ag on the silica surface was carried out without a catalyst in which only a few Ag^+ ions could be bonded to the silica surface. Research by Kim et al. (2007) on the deposition of silver particles on silica surfaces required the use of a catalyst and an alkaline condition. This involved deprotonation of the hydroxyl ligand in Si-OH and then the addition of a basic catalyst on Si-OH to produce a $Si\text{-}O^-$. Nucleophilic attack by SiO^- ions against electrophilic Ag^+ would subsequently occur and form Si-O-Ag. The study explained that the incorporation of Ag on the silica surface when without a catalyst showed only a tiny amount when compared by using a catalyst, even with the same concentration of Ag^+ source used. The following demonstrates the deposition reactions of silver particles on the surface of silica without and with the use of a catalyst.

Without catalyst

$$Si\text{-}O\text{-}H + Ag^+ \longrightarrow Si\text{-}O\text{-}Ag + H^+$$

With catalyst

$$Si\text{-}O\text{-}H + B: \longrightarrow Si\text{-}O^- + B\,H$$

$$Si\text{-}O^- + Ag^+ \longrightarrow Si\text{-}O\text{-}Ag \text{ (Kim et al., 2007)}$$

In accordance with the above-mentioned reactions, the addition of a catalyst would generate nucleophile (SiO^-) which would easily be bound to electrophilic metal (Ag^+). Ag^+ ions bonded to the silica surface can be found to be more in amount with a catalyst than without a catalyst. However, the present study did not involve the use of a catalyst in the process of adding Ag, leading to possible minor to no Ag that was bounded to SiO^-, and thus TF20+Ag was unable to inhibit bacterial growth.

Geothermal silica and $AgNO_3$ used in this study were micro-sized. $AgNO_3$ active agent was aimed to add antibacterial properties by generating Ag^+ ion nanoparticles. Silver nanoparticles are effective in inhibiting bacterial growth because of their ability to inactivate microorganism cells by damaging cell membranes and DNA replication. Silver in ionic form can stick well to the cell wall and enter the bacterial cytoplasm due to electrostatic interactions between silver ions and sulfur and phosphorus, which are components of bacterial protein and DNA. The interaction between silver ions and sulfur in membrane proteins causes cell membrane permeability to increase and inactivates respiratory enzymes. Enzyme inactivation will interfere with the respiration process which can provoke the formation of reactive oxygen species (ROS). The formation of ROS will damage or modify the sequence of deoxyribonucleic acid (DNA) bases. Therefore, the absorption of silver ions through the cell wall and then into the bacterial cytoplasm can cause death. Silver ions in cells will interfere with DNA replication, cell reproduction and even inactivate enzymes in the metabolic system (Yin, et all. 2020). Silver nanoparticles have a good ability to be adsorbed as they have a large surface area and smaller particle size. Small nanoparticles can easily enter bacterial cells (Zheng et al., 2018).

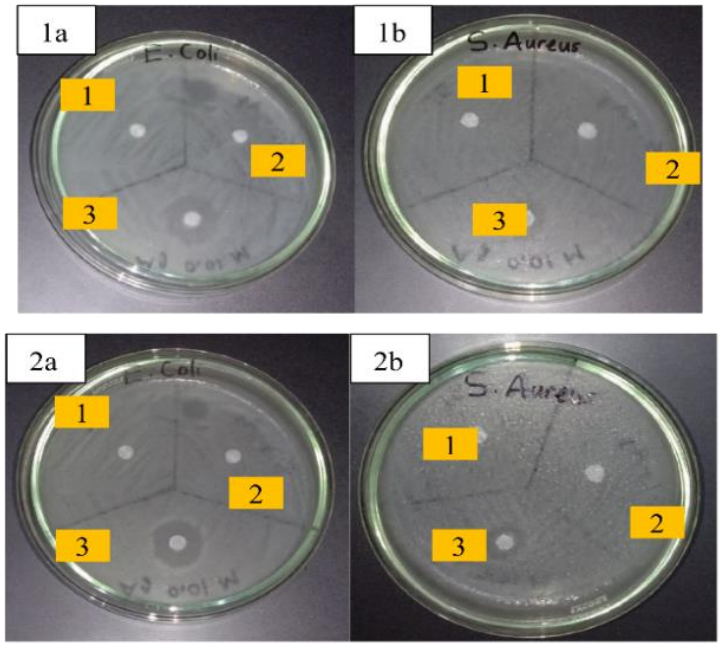

Figure 15. Inhibition zone results against (**a**) *E. Coli* (**b**) *S. Aureus* upon incubation for (**1**) 8 hours and (**2**) 12 hours. Description: (**1**) TF20, (**2**) TF20+Ag, (**3**) $AgNO_3$ 0.01M

CONCLUSIONS

Geothermal silica was purified using nitric acid (HNO_3). The optimum concentration of HNO_3 for the purification of geothermal silica waste was found to be 20%. Silica thin films were prepared from geothermal silica either without or with the addition of 0.01M $AgNO_3$. Silica thin films without or with the addition of $AgNO_3$ have contact angles of more than 150° (superhydrophobic) with FTIR characterization showing that the ratio of Si-O-Si area is greater than Si-OH based on deconvolution using Fityk. XRD results show that the silica thin films are amorphous, and Ag can deposit on the silica thin film material as demonstrated by SEM EDX. The antibacterial activity test of silica thin film without and with the addition of $AgNO_3$ shows no formation of inhibition zones against gram-negative bacteria (*Escherichia coli*) and gram-positive bacteria (*Staphylococcus aureus*), indicating that more research is needed to improve the antibacterial capabilities of the generated silica-thin films.

ACKNOWLEDGEMENTS

The authors would like to thank Faculty of Sciences and Mathematics, Universitas Diponegoro for financial support with grant number 2130/UN7.5.8.2/PP/2021.

REFERENCES

Afriani, F., Evi, J., Mahardika, R., Rafsanjani, R., & Tiandho, Y. (2019). Purification of silica from tin tailing by acid leaching methods. *Advances in Engineering Research, 167*, 5-7.

Brinker, C. J., & Scherer, G. W. (2013). *Sol-gel science: the physics and chemistry of sol-gel processing*: Academic press.

Bruni, S., Cariati, F., Casu, M., Lai, A., Musinu, A., Piccaluga, G., & Solinas, S. (1999). IR and NMR study of nanoparticle-support interactions in a Fe2O3-SiO2 nanocomposite prepared by a sol-gel method. *Nanostructured Materials, 11*(5), 573-586.

Darmawan, A., Rasyid, S. A., & Astuti, Y. (2021). Modification of the glass surface with hydrophobic silica thin layers using tetraethylorthosilicate (TEOS) and trimethylchlorosilane (TMCS) precursors. *Surface and Interface Analysis, 53*(3), 305-313.

Darmawan, A., Utari, R., Saputra, R. E., & Astuti, Y. (2018). Synthesis and characterization of hydrophobic silica thin layer derived from methyltrimethoxysilane (MTMS). In *IOP Conference Series: Materials Science and Engineering*, *299* (1), 012041). IOP Publishing.

De, G., Licciulli, A., Massaro, C., Tapfer, L., Catalano, M., Battaglin, G., Meneghini, C. and Mazzoldi, P. (1996). Silver nanocrystals in silica by sol-gel processing. *Journal of Non-Crystalline Solids, 194*(3), 225-234.

Esfahani, M.B., Eshaghi, A. and Bakhshi, S.R. (2022). Transparent hydrophobic, self-cleaning, anti-icing and anti-dust nano-structured silica based thin film on cover glass solar cell. *Journal of Non-Crystalline Solids*, *583*, 121479.

Epstein, I. R., Kustin, K., & Warshaw, L. J. (1980). A kinetics study of the oxidation of iron (II) by nitric acid. *Journal of the American Chemical Society, 102*(11), 3751-3758.

Fayomi, O., Akande, I., Abioye, O., & Fakehinde, O. (2019). New trend in thin film composite coating deposition: a mini review. *Procedia Manufacturing, 35*, 1007-1012.

Gao, M., Wang, Y., Zhang, Y., Li, Y., Tang, Y. and Huang, Y. (2020). Deposition of thin films on glass fiber fabrics by atmospheric pressure plasma jet. *Surface and Coatings Technology*, *404*, 126498.

Gurav, A. B., Xu, Q., Latthe, S. S., Vhatkar, R., Liu, S., Yoon, H., & Yoon, S. S. (2015). Superhydrophobic coatings prepared from methyl-modified silica particles using simple dip-coating method. *Ceramics International, 41*(2), 3017-3023.

Hemmatian T., Lee H., Kim J. (2021). Bacteria adhesion of textiles influenced by wettability and pore characteristics of fibrous substrates. *Polymers 13*, 223.

Javed, U., Farooq, R., Shehzad, F., & Khan, Z. (2018). Optimization of HNO_3 leaching of copper from old AMD Athlon processors using response surface methodology. *Journal of environmental management, 211*, 22-27.

Jenie, S. A., Ghaisani, A., Ningrum, Y. P., Kristiani, A., Aulia, F., & Petrus, H. T. (2018). Preparation of silica nanoparticles from geothermal sludge via sol-gel method. In *AIP Conference Proceedings, 2026* (1), 020008. AIP Publishing LLC.

Jeon, H.-J., Yi, S.-C., & Oh, S.-G. (2003). Preparation and antibacterial effects of Ag–SiO2 thin films by sol–gel method. *Biomaterials, 24*(27), 4921-4928.

Kasap, S., & Capper, P. (2017). *Springer handbook of electronic and photonic materials*: Springer.

Khalifa, M., Ouertani, R., Hajji, M., & Ezzaouia, H. (2019). Innovative technology for the production of high-purity sand silica by thermal treatment and acid leaching process. *Hydrometallurgy, 185*, 204-209.

Kim, Y. H., Lee, D. K., Cha, H. G., Kim, C. W., & Kang, Y. S. (2007). Synthesis and characterization of antibacterial $Ag-SiO_2$ nanocomposite. *The Journal of Physical Chemistry C, 111*(9), 3629-3635.

Kiomarsipour, N., Eshaghi, A., Ramazani, M., Zabolian, H. and Abbasi-Firouzjah, M. (2023). Preparation and evaluation of high-transparent scratch-resistant thin films on plasma treated polycarbonate substrate. *Arabian Journal of Chemistry*, *16*(5), 104667.

Lanje, A. S., Sharma, S. J., & Pode, R. B. (2010). Synthesis of silver nanoparticles: a safer alternative to conventional antimicrobial and antibacterial agents. *Journal of Chemical and Pharmaceutical Research*, *2*(3), 478-483.

Levana O., Hong S., Kim S.H., Jeong, J.H., Hur, S.S., Lee, J.W., Kwon, K.S. and Hwang, Y. (2022). A Novel strategy for creating an antibacterial surface using a highly efficient electrospray-based method for silica deposition. *International Journal of Molecular Sciences* 23, 513.

Li, J., Cao, J., Huo, L., & He, X. (2012). One-step synthesis of hydrophobic silica aerogel via in situ surface modification. *Materials Letters, 87*, 146-149.

Li, W., Seal, S., Megan, E., Ramsdell, J., Scammon, K., Lelong, G., . . . Richardson, K. A. (2003). Physical and optical properties of sol-gel nano-silver doped silica film on glass substrate as a function of heat-treatment temperature. *Journal of applied physics, 93*(12), 9553-9561.

Ma, B., Wang, C., Yang, W., Yang, B., & Zhang, Y. (2013). Selective pressure leaching of Fe (II)-rich limonitic laterite ores from Indonesia using nitric acid. *Minerals Engineering, 45*, 151-158.

Muljani, S., Setyawan, H., Wibawa, G., & Altway, A. (2014). A facile method for the production of high-surface-area mesoporous silica gels from geothermal sludge. *Advanced Powder Technology, 25*(5), 1593-1599.

Purnomo, A., Dalanta, F., Oktaviani, A. D., & Silviana, S. (2018). *Superhydrophobic coatings and self-cleaning through the use of geothermal scaling silica in improvement of material resistance*. In *AIP Conference Proceedings*, *2026* (1), 020077. AIP Publishing LLC.

Ramezani, M., Vaezi, M. R., & Kazemzadeh, A. (2015). The influence of the hydrophobic agent, catalyst, solvent and water content on the wetting properties of the silica films prepared by one-step sol–gel method. *Applied Surface Science, 326*, 99-106.

Rogozhnikov, D., Karimov, K., Shoppert, A., Dizer, O., & Naboichenko, S. (2021). Kinetics and mechanism of arsenopyrite leaching in nitric acid solutions in the presence of pyrite and Fe (III) ions. *Hydrometallurgy, 199*, 105525.

Safrianti, I., Wahyuni, N., & Zaharah, T. A. (2012). Adsorpsi timbal (II) oleh selulosa limbah jerami padi teraktivasi asam nitrat: pengaruh pH dan waktu kontak (Lead (II) adsorption by nitric acid-activated rice straw waste cellulose: influence of pH and contact time). *Jurnal Kimia Khatulistiwa, 1*(1).

Saputra, R. E., Astuti, Y., & Darmawan, A. (2018). Hydrophobicity of silica thin films: The deconvolution and interpretation by Fourier-transform infrared spectroscopy. *Spectrochimica Acta Part A: Molecular and Biomolecular Spectroscopy, 199*, 12-20.

Sarawade, P. B., Kim, J.-K., Hilonga, A., & Kim, H. T. (2010). Production of low-density sodium silicate-based hydrophobic silica aerogel beads by a novel fast gelation process and ambient pressure drying process. *Solid State Sciences, 12*(5), 911-918.

Sethi S.K., Manik G., (2018). Recent progress in super hydrophobic/hydrophilic self-cleaning surfaces for various industrial applications: a review. *Polymer-Plastics Technology and Engineering, 57*, 1932-52.

Shinde, Y., Sonone, P., & Ubale, A. (2020). Synthesis and characterization of hexagonal and tetrahedral nanocrystalline Sb_2O_3 thin films prepared by chemical spray pyrolysis technique. *Journal of Alloys and Compounds, 831*, 154777.

Silviana, S., Sanyoto, G. J., Darmawan, A., & Sutanto, H. (2020). Geothermal Silica Waste as Sustainable Amorphous Silica Source for The Synthesis of Silica Xerogels. *Rasayan J. Chem, 13*(3), 1692-1700.

Sotiriou, G. A., Teleki, A., Camenzind, A., Krumeich, F., Meyer, A., Panke, S., & Pratsinis, S. E. (2011). Nanosilver on nanostructured silica: Antibacterial activity and Ag surface area. *Chemical Engineering Journal, 170*(2-3), 547-554.

Sulejmanović, J., Memić, M., Huremović, J., & Selović, A. (2015). Simultaneous preconcentration and determination of Co (II), Cr (III), Fe (III), Mn (II), Ni (II) and Pb (II) by FAAS using silica gel modified with Niobium (V) oxide. *Chemical Science Review and Letters, 4*(14), 662-670.

Sumardi, A., Elma, M., Rampun, E.L.A., Lestari, A.E., Assyaifi, Z.L., Darmawan, A., Yanto, D.H.Y., Syauqiah, I., Mawaddah, Y. and Wati, L.S. (2021). Designing a mesoporous hybrid organo-silica thin film prepared from an organic catalyst. *Membrane Technology*, *2021*(2), 5-8.

Widiyandari, H., Pardoyo, P., Sartika, J., Putra, O., Purwanto, A., & Ernawati, L. (2021). Synthesis of mesoporous silica xerogel from geothermal sludge using sulfuric acid as gelation agent. *International Journal of Engineering, 34*(7), 1569-1575.

Yan, H., Yuanhao, W., & Hongxing, Y. (2017). TEOS/silane coupling agent composed double layers structure: A novel super-hydrophilic coating with controllable water contact angle value. *Applied Energy, 185*, 2209-2216.

Yin I.X., Zhang J., Zhao I.S., Mei M.L., Li Q., Chu C.H., (2020). The antibacterial mechanism of silver nanoparticles and its application in dentistry. *International journal of nanomedicine*, 2555-62.

Yuan Y., Hays M.P., Hardwidge P.R., Kim J., (2017). Surface characteristics influencing bacterial adhesion to polymeric substrates. *RSC advances 7*, 14254-61.